Supporting Information

Composition tuning of ultrafine cobalt-based spinel nanoparticles for efficient oxygen evolution

Jingbo Han,[a] Xiaohe Liu,[a,] Hao Wan,[a] Dan Wu,[a] Gen Chen,[a] Junhui Li,[a] Yijun Cao,[b] Renzhi Ma[c,]**

[a] School of Materials Science and Engineering, Central South University, Changsha, Hunan 410083, P.R. China.

[b] Henan Province Industrial Technology Research Institute of Resources and Materials, Zhengzhou University, Zhengzhou, Henan 450001, P. R. China.

[c] International Center for Materials Nanoarchitectonics (WPI-MANA), National Institute for Materials Science (NIMS), Tsukuba, Ibaraki 305-0044, Japan.

Corresponding author

*Email: liuxh@csu.edu.cn (X. Liu)

*Email: MA.Renzhi@nims.go.jp (R. Ma)

Number of pages: 14

Number of figures: 10

Number of tables: 5

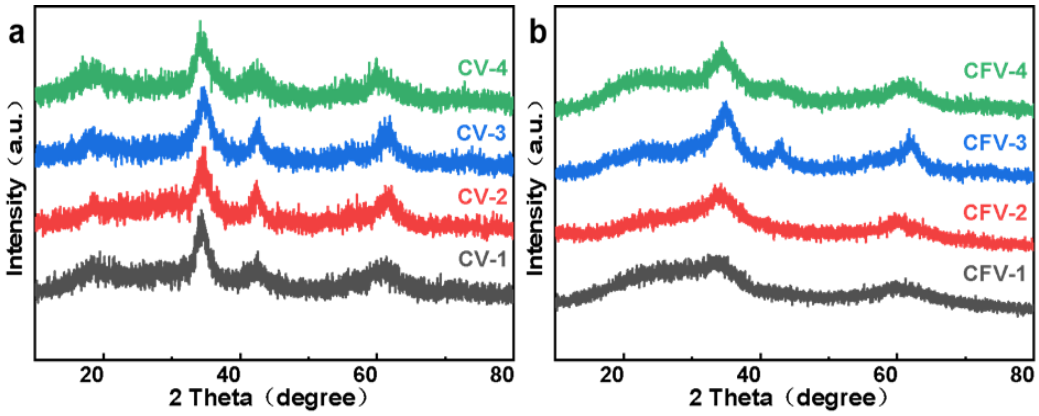

Figure S1. XRD patterns of (a) binary oxides (b) ternary oxides in different molar ratios.

Table S1. Composition analysis of the synthesized oxides by EDS.

Designed ratio (Co : Fe : V)	Practical ratio (Co : Fe : V)
1 : 0 : 0 (Co_3O_4)	1 : 0 : 0
2 : 0 : 1 (CV-1)	1.31 : 0 : 1
3 : 0 : 1 (CV-2)	1.88 : 0 : 1
5 : 0 : 1 (CV-3)	2.77 : 0 : 1
10 : 0 : 1 (CV-4)	4.49 : 0 : 1
2 : 1 : 1 (CFV-1)	1.49 : 1.24 : 1
3 : 1 : 1 (CFV-2)	1.83 : 1.13 : 1
5 : 1 : 1 (CFV-3)	2.81 : 0.94 : 1
10 : 1 : 1 (CFV-4)	4.68 : 1.19 : 1

Table S2. Interplanar spacings of 311 and 440 in synthesized Co_3O_4, CV-2 and CFV-2.

Catalyst	d_{311} (nm)	d_{440} (nm)	a (nm)
Co_3O_4	0.244	0.143	0.809
CV-2	0.257	0.150	0.851
CFV-2	0.262	0.155	0.872

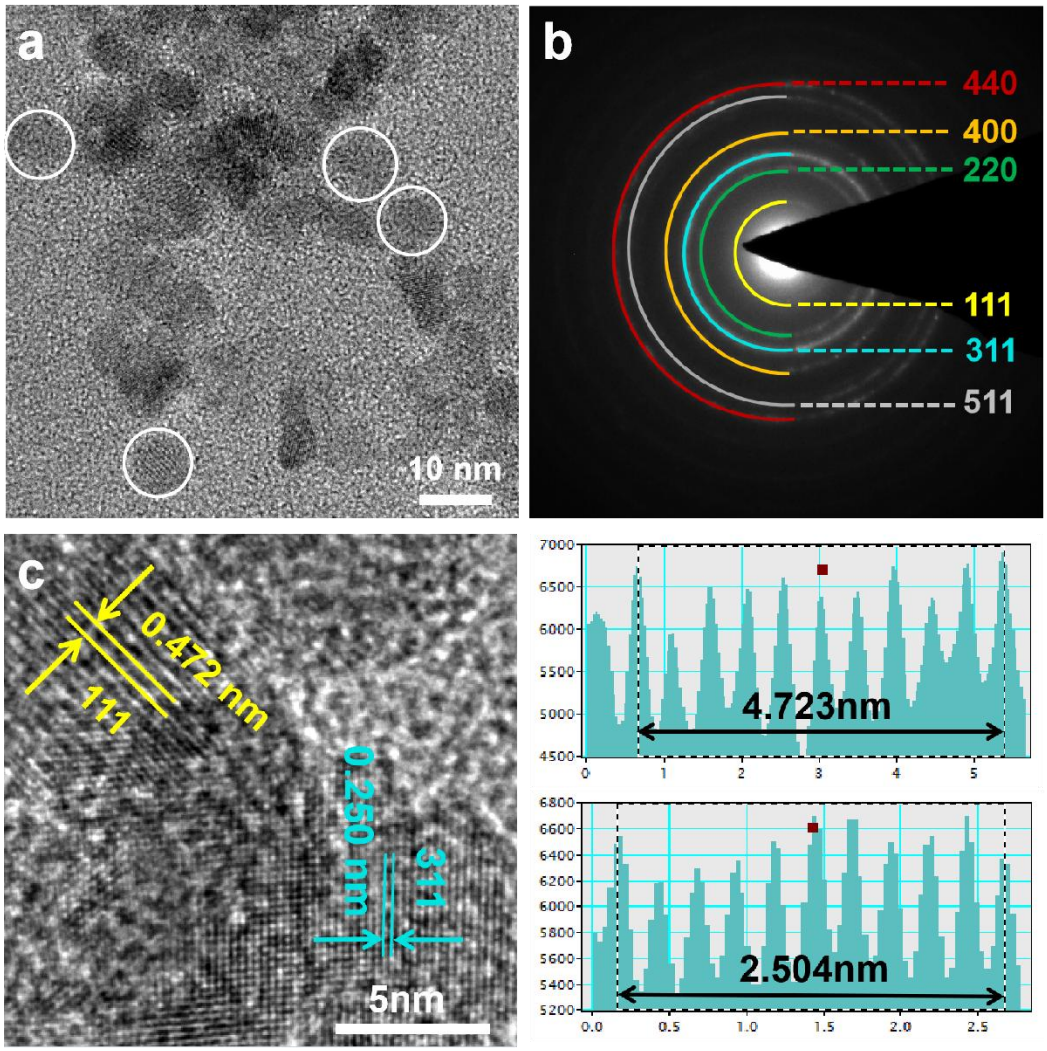

Figure S2. (a) TEM image (b) SAED pattern, (c) HRTEM image of as-synthesized Co_3O_4. The two different interplanar spacings coincide with those of 311 and 111 planes of Co_3O_4, respectively.

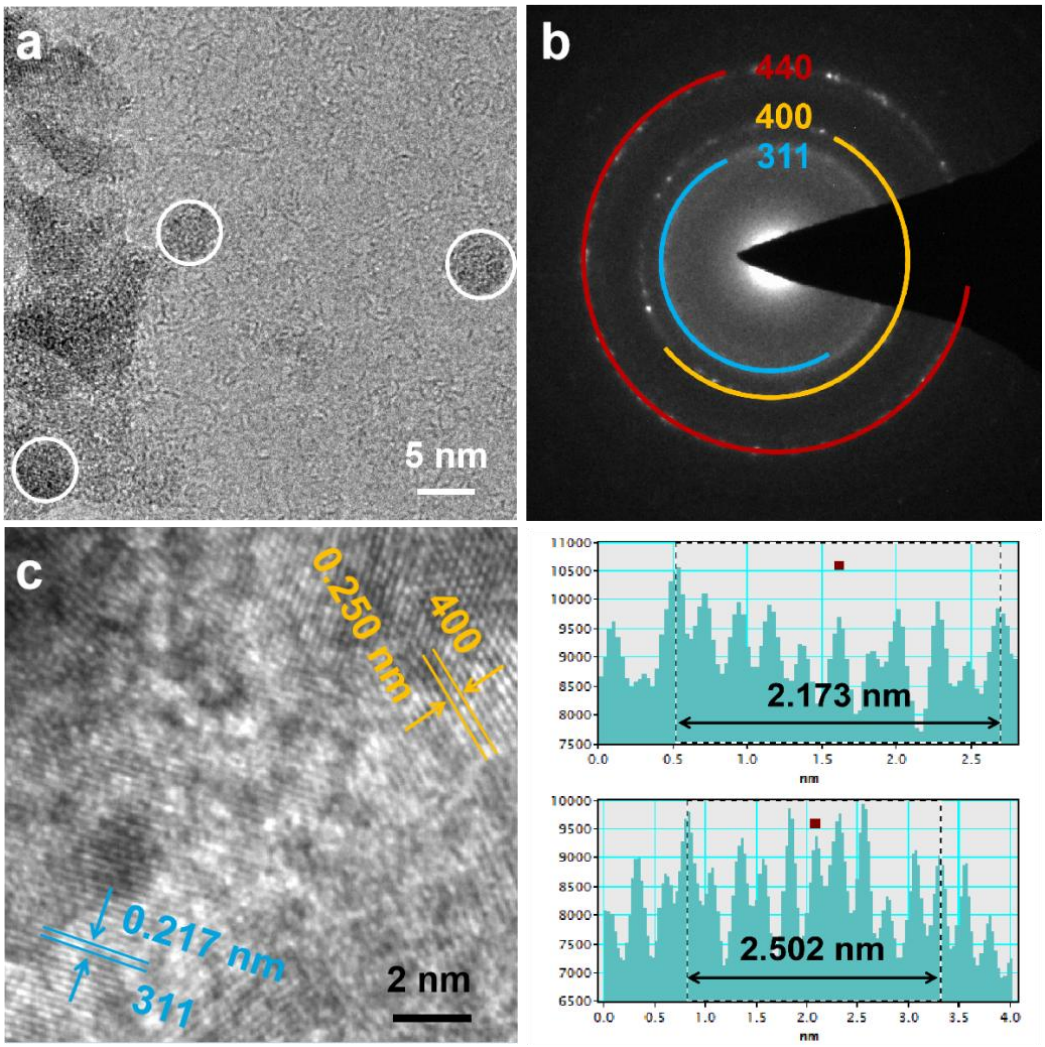

Figure S3. (a) TEM image (b) SAED pattern, (c) HRTEM image of as-synthesized CV-2. The two interplanar spacings in (c) respond to 311 and 400 planes of binary CoV spinel oxide, respectively.

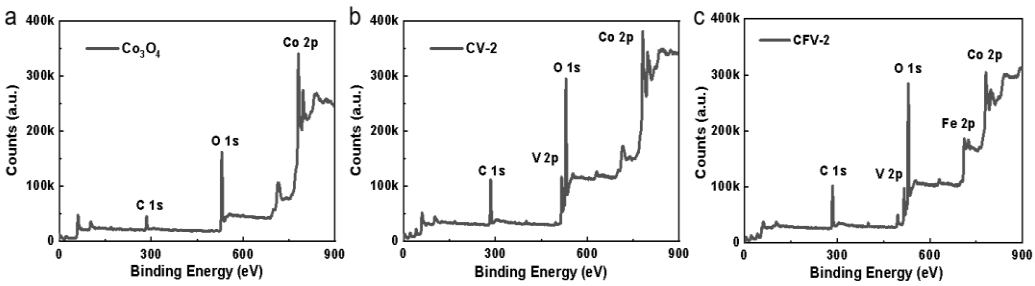

Figure S4. Wide-scan XPS spectra of (a) Co_3O_4 , (b) CV-2 and (c)CFV-2.

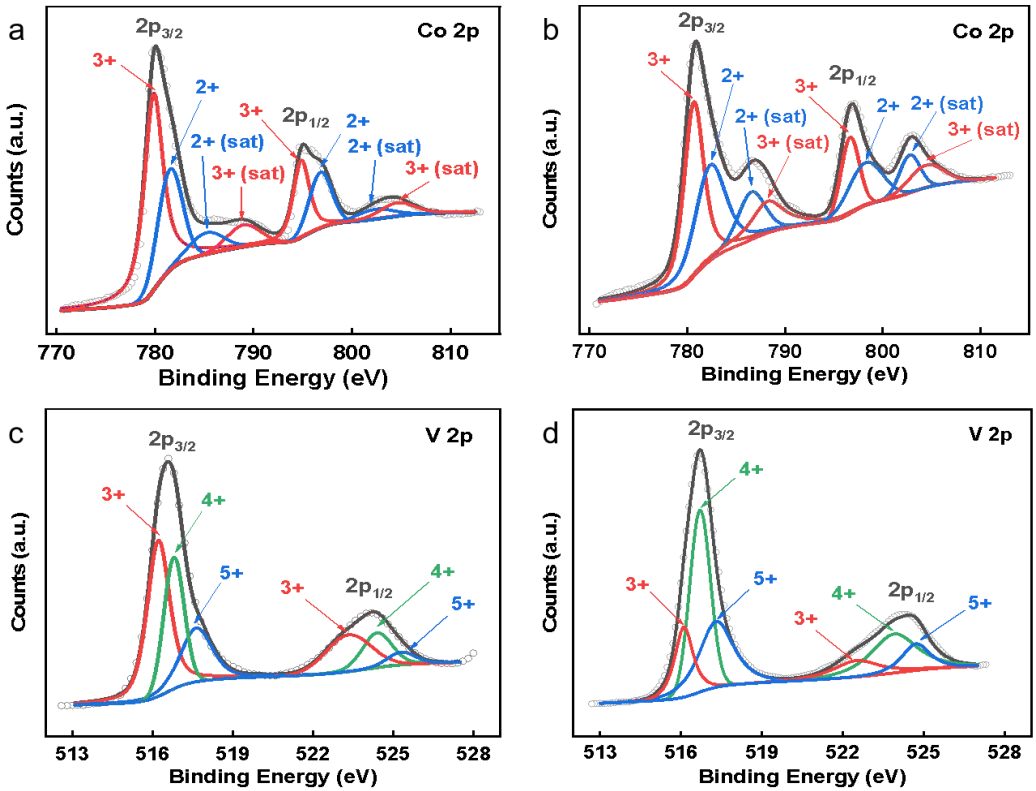

Figure S5. XPS spectra (a) Co 2p of Co_3O_4, (b) Co 2p of CV-2, (c) V 2p of CV-2 and (d) V 2p of CFV-2.

Table S3. Comparison of OER activity of as-synthesized oxides with reported electrocatalysts in the electrolyte of 1 M KOH .

Catalysts	Substrate	Overpotential	Tafel slope	Reference
$CoFeVO_4$	Glassy carbon	248 mV@10 mA cm^{-2}	52.8 mV dec^{-1}	This work
Co_2VO_4	Glassy carbon	295 mV@10 mA cm^{-2}	65.9 mV dec^{-1}	This work
Co_3O_4	Glassy carbon	316mV@10 mA cm^{-2}	78.6 mV dec^{-1}	This work
Co_3O_4/N-rmGO	Ni foam	310mV@10 mA cm^{-2}	67 mV dec^{-1}	[1]
reduced Co_3O_4	Glassy carbon	420mV@13.1 mA cm^{-2}	72 mV dec^{-1}	[2]
P-Co_3O_4	Ni foam	280mV@10 mA cm^{-2}	51.6 mV dec^{-1}	[3]
$Co_3V_2O_8$	Glassy carbon	359mV@10 mA cm^{-2}	65 mV dec^{-1}	[4]
reduced $CoFe_2O_4$ NS	Glassy carbon	320mV@10 mA cm^{-2}	48 mV dec^{-1}	[5]
CoFe-LDH	Ni foam	300mV@10 mA cm^{-2}	83 mV dec^{-1}	[6]
NiCoFe LTHs/CFC	Carbon fiber cloth	239mV@10 mA cm^{-2}	32 mV dec^{-1}	[7]
Fe-doped $NiCo_2O_4$	Ni foam	350mV@10 mA cm^{-2}	27 mV dec^{-1}	[8]
CoFeZr oxides/NF	Ni foam	264mV@20 mA cm^{-2}	54.2 mV dec^{-1}	[9]
NiV-LDH	Glassy carbon	318mV@10 mA cm^{-2}	50 mV dec^{-1}	[10]
NiFe-LDH/rGO	Glassy carbon	210mV@10 mA cm^{-2}	40 mV dec^{-1}	[11]
NiVFe-LDH	Ni foam	231mV@10 mA cm^{-2}	39.4 mV dec^{-1}	[12]
NiVFe-LDH	Ni foam	192mV@10 mA cm^{-2}	42 mV dec^{-1}	[13]
VOOH	Ni foam	270mV@10 mA cm^{-2}	68 mV dec^{-1}	[14]

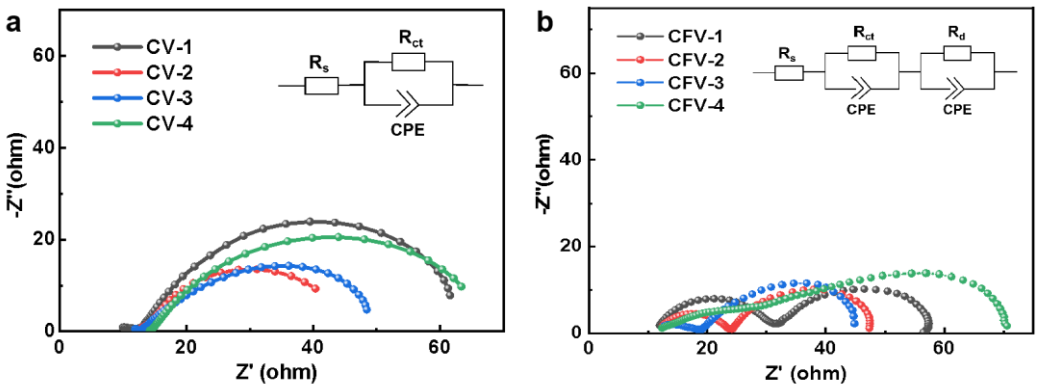

Figure S6. (a) EIS spectra of (a) binary oxides CV with different molar ratios, (b) ternary oxides CFV with different molar ratios. The inset of (a) and (b) are the corresponding equivalent circuits.

Table S4. The fitted values of resistances of R_s and R_{ct} of binary oxides.

Catalyst	R_s (Ω)	R_{ct} (Ω)
CV-1	12.0	52.3
CV-2	11.5	32.5
CV-3	11.1	39.8
CV-4	11.8	55.2

Table S5. The fitted values of resistances of R_s, R_{ct} and R_d of binary oxides.

Catalyst	R_s (Ω)	R_d(Ω)	R_{ct} (Ω)
CFV-1	11.2	19.9	28.5
CFV-2	11.6	12.2	24.0
CFV-3	10.9	13.1	26.9
CFV-4	10.6	22.8	34.6

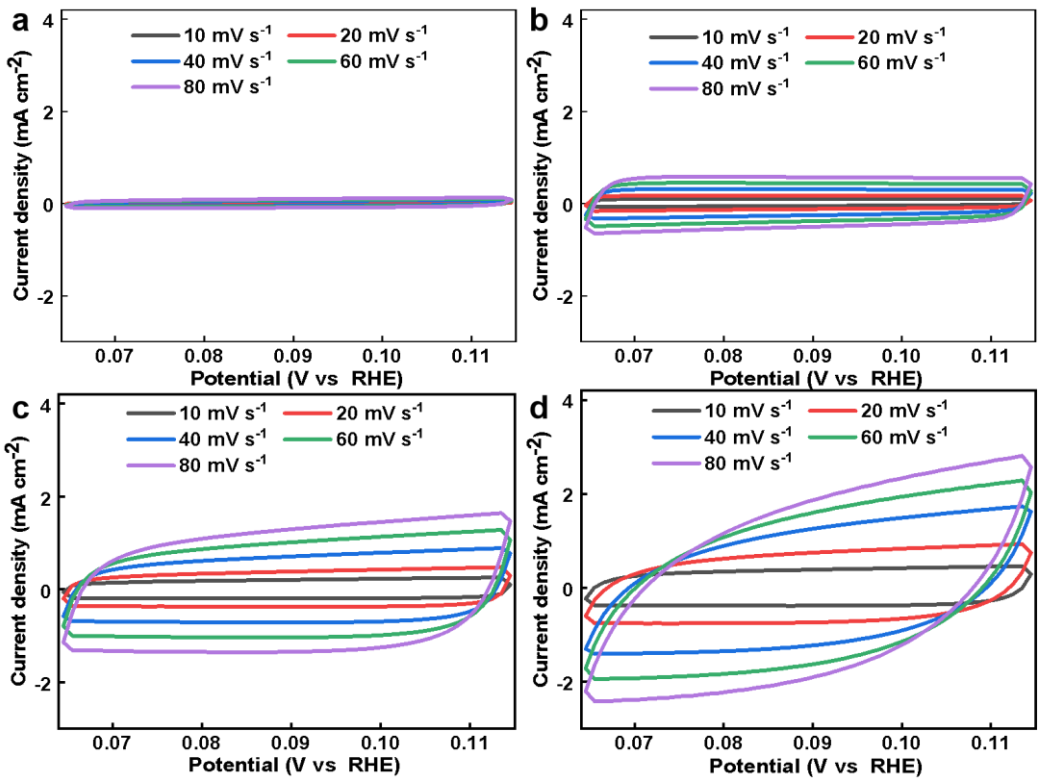

Figure S7. CV curves of (a) Co_3O_4 (b) RuO_2 (c) CV-2 (d) CFV-2 at incremental scan rates.

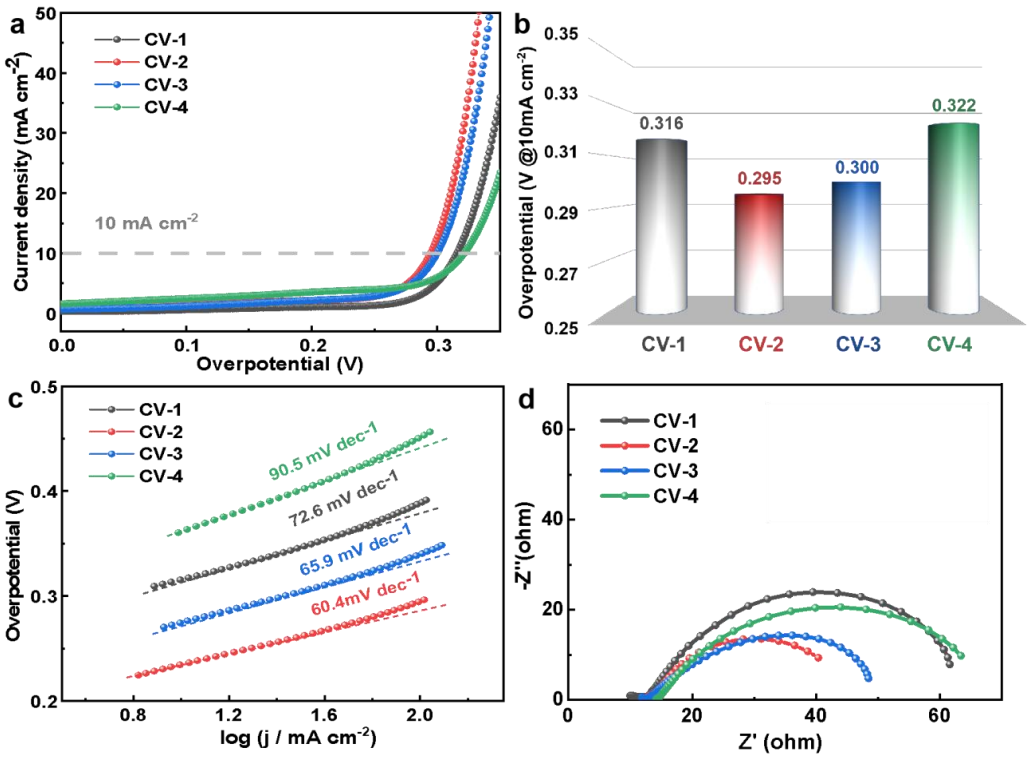

Figure S8. (a) LSV curves (b) Histogram of overpotential at 10 mA cm^{-2} (c) Tafel slopes (d) EIS spectra of binary oxides CV with different molar ratios.

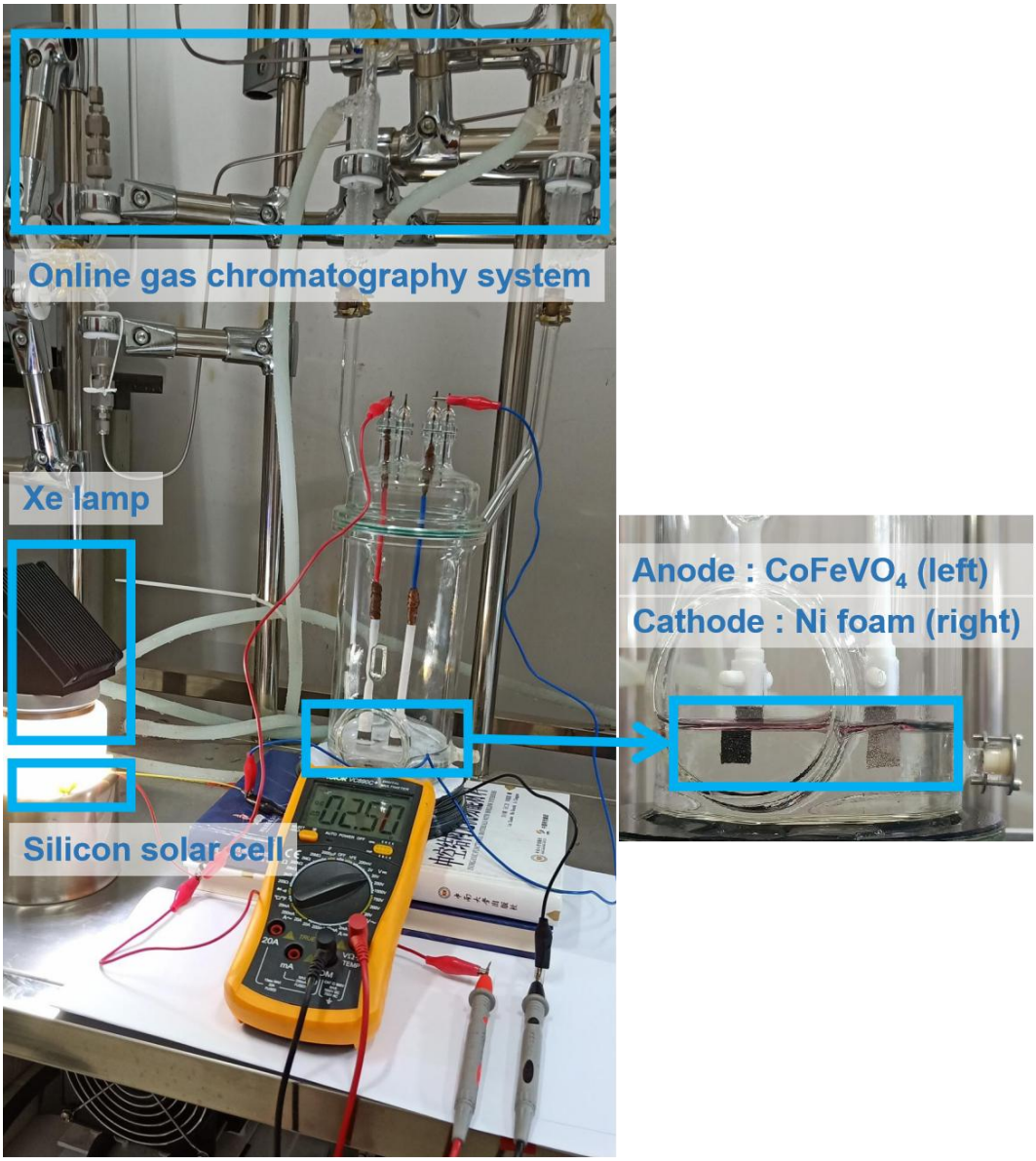

Figure S9. The photograph of the device.

Faraday efficiency was defined as the ratio between the actual and theoretical amount of the product. The total charge ($Q = I \times t$) passed during the reaction was divided by $n \times F$ (n is the number of electron transfer, F is the Faraday constant) to get the theoretical gas yield. m is the actual moles of the product (6122.5 μmol during the first 1.5 hour). The calculation process for the Faraday efficiency is as following:

Faraday Efficiency = actual gas yield / theoretical gas yield = $m / [(I \times t) / (n \times F)] = (m \times n \times F) / (I \times t) = (6122.5 \times 10^{-6}\ \text{mol} \times 2 \times 96485\ \text{C mol}^{-1}) / (224 \times 10^{-3}\ \text{A} \times 5400\ \text{s}) = 97.7\%$.

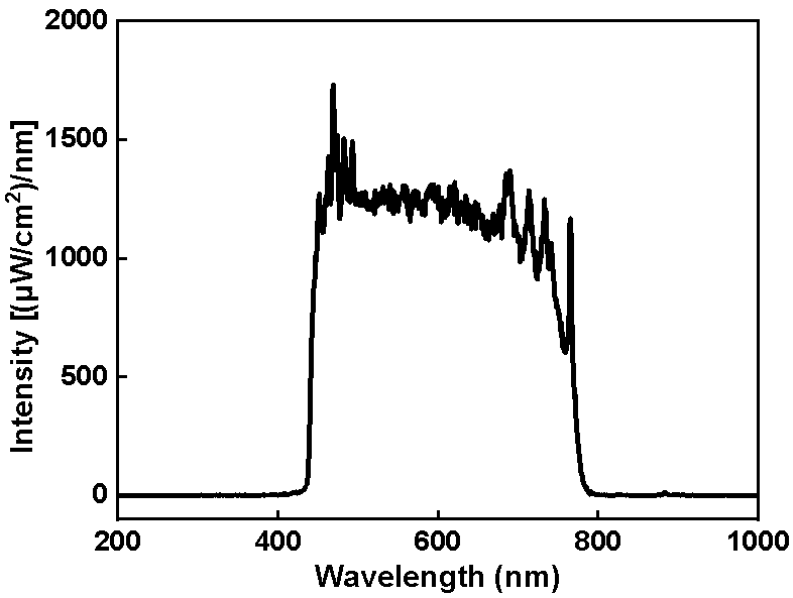

Figure S10. Irradiative spectrum of the Xe lamp (the major intensity is concentrated on the range of 400 nm < λ < 800 nm).

The average integral light intensity measured by the light meter is 0.3887 W cm^{-2}. The irradiated area for the silicon solar cell is 14.4 cm^2. The standard molar enthalpy of combustion for H_2 is -285.84 kJ mol^{-1}. The yield of H_2 during the first 1.5 hour is 6122.5 μmol. The calculation steps are as following:

Input: Solar energy (J) = light intensity (W cm^{-2}) × illumination area (cm^2) × time (s) = 0.3887 W cm^{-2} × 14.4 cm^2 × 5400 s = 30.2253 kJ

Output: H_2 energy (kJ) = standard molar enthalpy of combustion (kJ mol^{-1}) × H_2 moles (mol) = 285.84 kJ mol^{-1} × 6122.5 × 10^{-6} mol = 1.7501 kJ

Solar-to-Hydrogen energy conversion efficiency = H_2 energy (kJ) / Solar energy (kJ) = 1.7501 / 30.2253 = 5.8%

References

(1) Liang, Y., Li, Y., Wang, H., Zhou, J., Wang, J., Regier, T., Dai, H. Co_3O_4 nanocrystals on graphene as a synergistic catalyst for oxygen reduction reaction. *Nat. Mater.* **2011**, 10(10), 780-786, DOI 10.1038/nmat3087.

(2) Wang, Y., Zhou, T., Jiang, K., Da, P., Peng, Z., Tang, J., Zheng, G. Reduced mesoporous Co_3O_4 nanowires as efficient water oxidation electrocatalysts and supercapacitor electrodes. *Adv. Energy Mater.* **2014**, 4(16), 1400696, DOI 10.1002/aenm.201400696.

(3) Xiao, Z., Wang, Y., Huang, Y. C., Wei, Z., Dong, C. L., Ma, J., Wang, S. Filling the oxygen vacancies in Co_3O_4 with phosphorus: an ultra-efficient electrocatalyst for overall water splitting. *Energy Environ. Sci.* **2017**, 10(12), 2563-2569, DOI 10.1039/c7ee01917c.

(4) Xing, M., Kong, L. B., Liu, M. C., Liu, L. Y., Kang, L., Luo, Y. C. Cobalt vanadate as highly active, stable, noble metal-free oxygen evolution electrocatalyst. *J. Mater. Chem. A* **2014**, 2(43), 18435-18443, DOI 10.1039/C4TA03776F.

(5) Yan, K., Shang, X., Liu, Z., Dong, B., Lu, S., Chi, J., Gao, W., Chai, Y., Liu, C. A facile method for reduced $CoFe_2O_4$ nanosheets with rich oxygen vacancies for efficient oxygen evolution reaction. *Int. J. Hydrogen Energy* **2017**, 42(38), 24150-24158, DOI 10.1016/j.ijhydene.2017.07.165.

(6) Feng, L., Li, A., Li, Y., Liu, J., Wang, L., Huang, L., Ge, X. A highly active CoFe layered double hydroxide for water splitting. *ChemPlusChem* **2017**, 82(3), 483-488, DOI 10.1002/cplu.201700005.

(7) Wang, A. L., Xu, H., Li, G. R. NiCoFe layered triple hydroxides with porous structures as high-performance electrocatalysts for overall water splitting. *ACS Energy Lett.* **2016**, 1(2), 445-453, DOI 10.1021/acsenergylett.6b00219.

(8) Yan, K. L., Shang, X., Li, Z., Dong, B., Li, X., Gao, W. K., Liu, C. G. Ternary mixed metal Fe-doped $NiCo_2O_4$ nanowires as efficient electrocatalysts for oxygen evolution reaction. *Appl. Surf. Sci*. **2017**, 416, 371-378, DOI 10.1016/j.apsusc.2017.04.204.

(9) Huang, L., Chen, D., Luo, G., Lu, Y. R., Chen, C., Zou, Y., Wang, S. Zirconium-Regulation-Induced Bifunctionality in 3D Cobalt-Iron Oxide Nanosheets for Overall Water Splitting. *Adv. Mater.* **2019**, 28(31), 1901439, DOI 10.1002/adma.201901439.

(10) Fan, K., Chen, H., Ji, Y., Huang, H., Claesson, P. M., Daniel, Q., Sun, L. Nickel-vanadium monolayer double hydroxide for efficient electrochemical water oxidation. *Nat. Commun.* **2016**, 7, 11981, DOI 10.1038/ncomms11981.

(11) Ma, W., Ma, R., Wang, C., Liang, J., Liu, X., Zhou, K., Sasaki, T. A superlattice of alternately stacked Ni-Fe hydroxide nanosheets and graphene for efficient splitting of water. *ACS Nano* **2015**, 9(2), 1977-1984, DOI 10.1021/nn5069836.

(12) Dinh, K. N., Zheng, P., Dai, Z., Zhang, Y., Dangol, R., Zheng, Y., Yan, Q. Ultrathin porous NiFeV ternary layer hydroxide nanosheets as a highly efficient

bifunctional electrocatalyst for overall water splitting. *Small* **2018**, 14(8), 1703257, DOI 10.1002/smll.201703257.

(13) Li, P., Duan, X., Kuang, Y., Li, Y., Zhang, G., Liu, W., Sun, X. Tuning electronic structure of NiFe layered double hydroxides with vanadium doping toward high efficient electrocatalytic water oxidation. *Adv. Energy Mater.* **2018**, 8(15), 1703341, DOI 10.1002/aenm.201703341.

(14) Shi, H., Liang, H., Ming, F., Wang, Z. Efficient Overall Water-Splitting Electrocatalysis Using Lepidocrocite VOOH Hollow Nanospheres. *Angew. Chem. Int. Ed.* **2017**, 56(2), 573-577, DOI 10.1002/anie.201610211.